Research Article

Wen-Guang Zhou, Yu-Chen Leng, Li-Xiang Liu, Ming-Ming Yang, Wei Liu, Jing-Lan Liu, Pei Zhao, Yi Liu, Long-Long Wang, Ya-Xuan Shang, Xiao-Li Li*, Xiao-Hui Zhao*, Xue-Lu Liu* and Yang Xu*

Twist angle dependent absorption feature induced by interlayer rotations in CVD bilayer graphene

https://doi.org/10.1515/nanoph-2021-0190
Received April 26, 2021; accepted June 29, 2021;
published online July 19, 2021

Abstract: Bilayer graphene (BLG) grown via chemical vapor deposition (CVD) tends to exhibit twisted stacking. The twist angle θ_t in twisted BLG (tBLG) provides a new degree of freedom for engineering its electronic and optical properties. In this paper, we investigate the θ_t-dependent optical absorption in tBLG and deeply understand the electronic structure-optical properties correlations. New absorption peaks, whose wavelengths are modified by θ_t, are observed on the feature of optical contrast (OC) in tBLG. Under the corresponding energy excitation, the Raman G mode in tBLG exhibits a significant enhancement. Furthermore, the results of θ_t obtained by OC absorption peak are verified to be consistent with those by the Raman R mode. All these properties are proved to be related to the energy difference between low-energy Van Hove singularities (E_{VHS}) in the density of states of tBLGs. This work builds a relation between optical absorption and twist angle, providing a viable method to identifying twist angles in tBLGs.

Keywords: bilayer graphene; optical contrast; Raman spectra; twist angle.

1 Introduction

The large-area and high-quality graphene films grown via chemical vapor deposition (CVD) have been of particular interest in the technological and practical applications due to its simplicity and cost effectiveness. Recent experiments have shown that CVD-grown bilayer graphene (BLG) (CVD-BLG) tends to exhibit twisted stacking, i.e., twisted

Wen-Guang Zhou, Yu-Chen Leng, Li-Xiang Liu, and Ming-Ming Yang contributed equally to this work.

***Corresponding authors: Xiao-Li Li and Xiao-Hui Zhao**, National-Local Joint Engineering Laboratory of New Energy Photoelectric Devices & Hebei Key laboratory of Optic-electronic Information and Materials, College of Physics Science and Technology, Hebei University, Baoding 071002, China, E-mail: xiaolili@hbu.edu.cn (X.-L. Li), xhzhao123@163.com (X.-H. Zhao). https://orcid.org/0000-0001-8280-0877 (X.-L. Li); and **Xue-Lu Liu**, State Key Laboratory of Superlattices and Microstructures, Institute of Semiconductors, Chinese Academy of Sciences, Beijing 100083, China, E-mail: liuxuelu@semi.ac.cn; and **Yang Xu**, Colleges of ISEE and Microelectronics, State Key Laboratories of Modern Optical Instrumentation and Silicon Materials, Hangzhou Global Scientific and Technological Innovation Center, ZJU-UIUC Joint Institute,Zhejiang University, Hangzhou 310027, China, E-mail: yangxu-isee@zju.edu.cn

Wen-Guang Zhou, Ming-Ming Yang, Yi Liu and Long-Long Wang, National-Local Joint Engineering Laboratory of New Energy Photoelectric Devices & Hebei Key laboratory of Optic-electronic Information and Materials, College of Physics Science and Technology, Hebei University, Baoding 071002, China, E-mail: zhouwenguang@semi.ac.cn (W.-G. Zhou), 18803276272@163.com (M.-M. Yang), LIUYI763374220@163.com (Y. Liu), 3361289613@qq.com (L.-L. Wang)

Yu-Chen Leng, State Key Laboratory of Superlattices and Microstructures, Institute of Semiconductors, Chinese Academy of Sciences, Beijing 100083, China; and Center of Materials Science and Optoelectronics Engineering & CAS Center of Excellence in Topological Quantum Computation, University of Chinese Academy of Sciences, Beijing 100049, China, E-mail: ycleng@semi.ac.cn

Li-Xiang Liu and Wei Liu, Colleges of ISEE and Microelectronics, State Key Laboratories of Modern Optical Instrumentation and Silicon Materials, Hangzhou Global Scientific and Technological Innovation Center, ZJU-UIUC Joint Institute, Zhejiang University, Hangzhou 310027, China, E-mail: 11731032@zju.edu.cn (L.-X. Liu), liuv-isee@zju.edu.cn (W. Liu)

Jing-Lan Liu and Pei Zhao, Center for X-Mechanics and Institute of Applied Mechanics, Zhejiang University, Hangzhou 310027, China, E-mail: jinglanliu@zju.edu.cn (J.-L. Liu), peizhao@zju.edu.cn (P. Zhao)

Ya-Xuan Shang, State Key Laboratory of Superlattices and Microstructures, Institute of Semiconductors, Chinese Academy of Sciences, Beijing 100083, China, E-mail: yaxuanhd@semi.ac.cn

BLG (tBLG) [1], in which one single-layer graphene (SLG) rotates by a twist angle, θ_t, relative to the other. In tBLGs, the constituent SLGs couple with each other and form Moire patterns with a longer period [2, 3], producing a unique band structure [4, 5] which is different from that of the individual constituents and from that expected for pristine BLG. As a result, novel physical properties emerge in tBLGs, such as Dirac-like linear dispersion with lower Fermi velocity than that in SLG [4], new Van Hove singularities (VHSs) [5] in the low-energy electronic density of states, and correlated insulator and superconductivity behaviors in magic-angle tBLG [6, 7]. These properties provide the possibility of potential optoelectronic devices with multiple degrees of freedom, and thus it is essential to understand θ_t-property correlations in tBLGs. Although Raman spectroscopy of tBLG has provided evidence of intriguing θ_t-dependent optical properties [8, 9], these studies are not comprehensive enough to generalize tBLG with diverse θ_t because it is time-consuming and difficult to determine θ_t for a rapid measurement over a large area of samples. Therefore, how to find a universal and fast method to identify θ_t-dependent tBLG flakes by CVD is still an open and essential issue. Notably, the unique band structure could lead to additional optical features in optical conductivity of tBLGs [10, 11], and even the gate-driven evolution of optical features and band structures was further studied [11]. In addition, transitions between parallel electronic bands across the Fermi level in tBLGs could also generate θ_t-dependent optical absorption peaks [9, 12]. These provided an ideal platform by optical methods to study θ_t in tBLGs.

Here, we proposed a rapid and efficient optical method to allow simultaneous θ_t identification and interlayer coupling studies in tBLGs with high spatial resolution. Because the optical absorption is significantly selectively enhanced due to the θ_t-dependent change of energy difference between VHSs in tBLGs [12], our method relies on a wavelength dependent absorption peak appearing on the feature of OC between the reflection spectra from tBLG supported by SiO_2/Si substrate and from the bare SiO_2/Si substrate. Using exfoliated BLG (ex-BLG) as a standard reference, tBLGs with diverse θ_t in CVD-BLG can be identified by wavelength-related absorption peaks of OC. In this letter, a white light source (with excitation range from 400 to 800 nm) is used in the OC experiments and all the tBLGs with absorption peak wavelength from 400 to 800 nm are summarized. The corresponding θ_t of tBLGs were calculated by energy difference related to low-energy saddle-point excitons. The θ_t-related optical properties of these tBLGs were also exhibited by Raman spectroscopy. The enhanced G modes can be seen in tBLGs when the excitation lasers are coincident with the absorption peaks. Moreover, a series of R modes of tBLGs can be detected under the excitation associated with the absorption peak. By analyzing the R modes, θ_t of tBLGs can be verified.

2 Experimental methods

2.1 Sample preparation

The exfoliated SLG (ex-SLG) and ex-BLG as the references used in this work were mechanically exfoliated from a highly oriented pyrolytic graphite (HOPG) onto the 90 nm SiO_2/Si substrate. The layer number of the ex-BLG and ex-SLG were determined by the line shape of 2D band [13] in Raman spectra excited with a 633 nm laser, which were shown in Figure S1 of Supplementary Materials.

The CVD-grown graphene samples were grown on annealed copper substrate (Alfa Aesar #46365, purity of 99.8%, and thickness of 25 μm) in a low-pressure chemical vapor deposition (LPCVD, Thermo Scientific Lindberg/Blue M) system with a tube furnace (inner diameter of 50 mm). Firstly, the LPCVD system was evacuated to 0.5 Pa, and then the Cu substrate was annealed at 1060 °C for 100 min under 50 sccm H_2 with a pressure of about 50 Pa. One additional step was also adopted by flowing 1 sccm O_2 for 10 min to reduce the nucleation density. With the slight incorporation of the oxygen on the Cu surface, the flakes grow under the typical condition of 300 sccm H_2 and 0.3 sccm CH_4. After 3-h growth, the system was cooled down to room temperature with the gas flowing. The graphene grown on the reverse side of Cu foil was etched by O_2 plasma. After etching, poly(methyl methacrylate) (PMMA) was spin-coated (with 1000 rpm for 10 s and then 4000 rpm for 60 s) on graphene/Cu. Then the PMMA/graphene/Cu was put into the Cu etchant ($CuSO_4 \cdot 5H_2O$:HCl:H_2O = 15.6 g:50 mL:50 mL) for 4 h to obtain the PMMA/graphene film. And then the film was rinsed in deionized (DI) water for 5 min to remove the Cu particles and polymer residuals. PMMA/graphene was then transferred onto a 90 nm SiO_2/Si substrate (same with the substrates used on ex-SLG and ex-BLG). Finally, the PMMA was washed off using dichloromethane (DCM) at 50 °C and isopropyl alcohol (IPA). The CVD-SLG and CVD-BLG were found as an external hexagon (with one layer) and an internal one (with two layers) respectively in an optical microscope. Their layer number was determined by the feature of OC with ex-SLG and ex-BLG as the references. It will be described in more detail in Section 3.1.

2.2 OC and Raman measurements

Reflection spectra were performed in a backscattering geometry using an HR Evolution micro-Raman system. The tungsten halogen lamp was used as a light source with the spot size below 2 μm. A 100× objective lens (NA = 0.9) was used to ensure the accuracy of tests with the size of samples above 2 μm. The best reflected light signal was achieved by focusing the microscope to get maximum peak intensity. The reflection spectra were measured from the samples and bare substrates in the broad wavelength range of 400–800 nm. The 600 lines/mm grating was used, which enables one to have each CCD pixel to cover 1 nm. We used $R_{sam+sub}(\lambda)$ and $R_{sub}(\lambda)$ to respectively indicate the reflection intensities of samples and bare substrates and used the OC method to normalize the data by the formula of $OC(\lambda) = 1 - R_{sam+sub}(\lambda)/R_{sub}(\lambda)$. Raman spectra were also performed in a backscattering geometry using the HR Evolution micro-Raman system with the 100× objective lens (NA = 0.9). The lasers used in measurements were 2.71, 2.54, 2.33, 2.09, 1.96, and 1.83 eV, respectively. The 1800 lines/mm grating was used, and the achieved spectral resolution was about 0.5 cm^{-1}. During all the measurements, laser power has been kept below 300 μW to prevent any sample heating. The integration time of 50 s was adopted to ensure a good signal-to-noise ratio.

3 Results and discussions

3.1 Optical contrast of ex-SLG, ex-BLG, CVD-SLG, and CVD-BLG

The SLG is a typical two-dimensional system with in-plane atoms coupled by strong covalent bonds to form sp^2 carbon hexagonal networks. The BLG is stacked by two SLGs connected by weak van der Waals (vdW) interactions. The BLG produced by mechanical exfoliation of HOPG is almost exclusively Bernal-stacked. The optical images of ex-SLG and ex-BLG were shown in Figure 1a and the measured OC(λ) of ex-SLG and ex-BLG were plotted by grey lines in Figure 1c with the wavelength ranging from 400 to 800 nm. Both of ex-SLG and ex-BLG exhibit large and wide absorption features, and the maximum value of OC(λ) of ex-BLG is apparently larger than those of ex-SLG with the offset about 12%, which is consistent with previous reports [14]. The optical images of CVD-SLG and CVD-BLG were shown in Figure 1b, in which even more layers were contained. The OC(λ) of CVD-SLG was plotted by red line in Figure 1c, which basically matched the OC(λ) of ex-SLG because the CVD-SLG were transferred to the same SiO_2/Si substrates with ex-SLG. The OC(λ) of CVD-BLG was plotted by blue line in Figure 1c. There is a broad background centered around 560 nm in the OC(λ) of both ex-BLG and CVD-BLG samples, and the broad outlines of two curves coincide roughly. However, the area enclosed by the red circle in Figure 1b was identified as a tBLG with a specific θ_t due to an additional absorption peak appearing at ~542 nm in the OC(λ) which was different from that of ex-BLG. By comparing the OC between the tBLG and ex-BLG, the θ_t-related narrow absorption peak of tBLG was exhibited; we took the position of the maximum as the position of the absorption peak. Thus, when white-light of a microscope is incident from air onto tBLG on SiO_2/Si substrate, the peculiar physical properties dependent on θ_t of tBLG can be seen by the modification of the reflected light intensity from tBLG relative to that directly from the bare substrates due to the optical enhancement effect from multiple reflections at the interfaces and optical interference within tBLG and substrate.

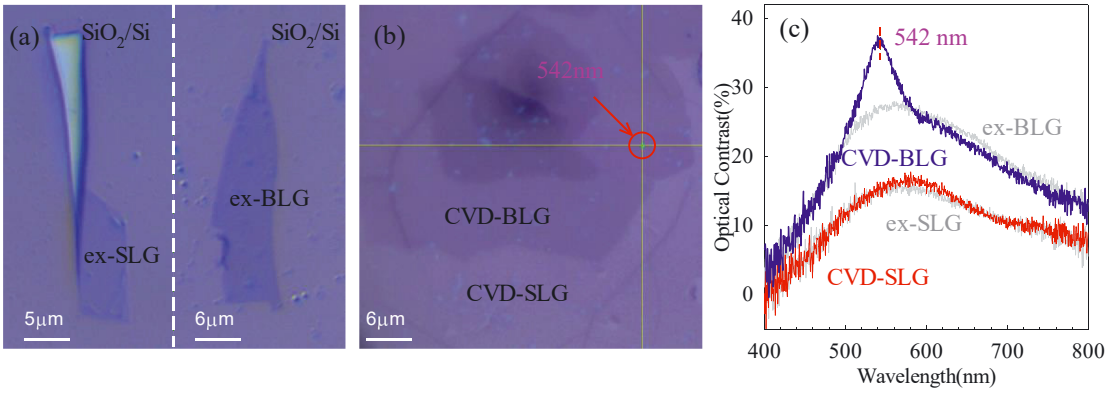

Figure 1: (a) Optical images of ex-SLG and ex-BLG, (b) optical images of CVD-SLG and CVD-BLG, where the area plotted by the red circle is tBLG. (c) The optical contrast ($OC(\lambda) = 1 - R_{sam+sub}(\lambda)/R_{sub}(\lambda)$) of ex-SLG, ex-BLG, CVD-SLG, and tBLG (indicated in (b)) with the wavelength ranging from 400 to 800 nm.

3.2 The relationship between the absorption peak in OC(λ) and twist angle θ_t

The larger area of CVD-grown sample is, the more complex its stacking order is. In order to investigate the relationship between the absorption peak wavelength and the twist angle θ_t, we recorded the OC(λ) of multiple CVD-BLG samples. The OC(λ) of 24 tBLGs with different absorption peak wavelength from 400 nm to 800 nm were shown in Figure 2a and b. In order to distinguish each OC(λ) clearly, the interval between adjacent spectral lines is artificially set at 10% increments. The absorption peak appears in 418 nm with the shortest wavelength and in 774 nm with the longest wavelength. These absorption peaks are due to novel electronic states because of electron coupling between layers when the upper and lower layers have relative twist. The coupling and interaction of electrons between layers depend largely on the distortion between the individual atomic lattices in each layer, which constitute the periodic superlattice of tBLG [15]. The period size of periodic superlattice depends entirely on the twist angles between the upper and lower layers, giving tBLG controllable optical properties. P. Moon et al. [16] firstly theoretically investigated the absorption peaks of tBLGs and associated these absorption peaks with the strong VHSs induced by the quasi-periodic Moiré cell, pointing out that these absorption peaks could serve as a fingerprint to identify the twist angle. The energy difference between the low-energy VHSs, i.e., E_{VHS}, in the joint density of states (JDOS) of tBLGs, satisfies the following angular dependence which were calculated by H. B. Ribeiro et al. [17],

$$E_{VHS}\,(\mathrm{eV}) = (8\pi\hbar v_F/3a)\sin(\theta t/2),$$

where θt is the twist angle between two layers, $\hbar$ is the reduced Planck's constant, a and v_F are, respectively, the lattice parameter ($a = 2.46 \times 10^{-10}$m) and the Fermi velocity of SLG. Here, we set $v_F = (0.80 \pm 0.06) \times 10^6$m/s [17] regardless of the departure of the linear electronic dispersion at the crossing of the bottom and top layer Dirac cones. When the wavelength of absorption peak was converted to the energy corresponding to E_{VHS} by $E_{VHS}\,(\mathrm{eV}) = 1240/\lambda\,(\mathrm{nm})$, we

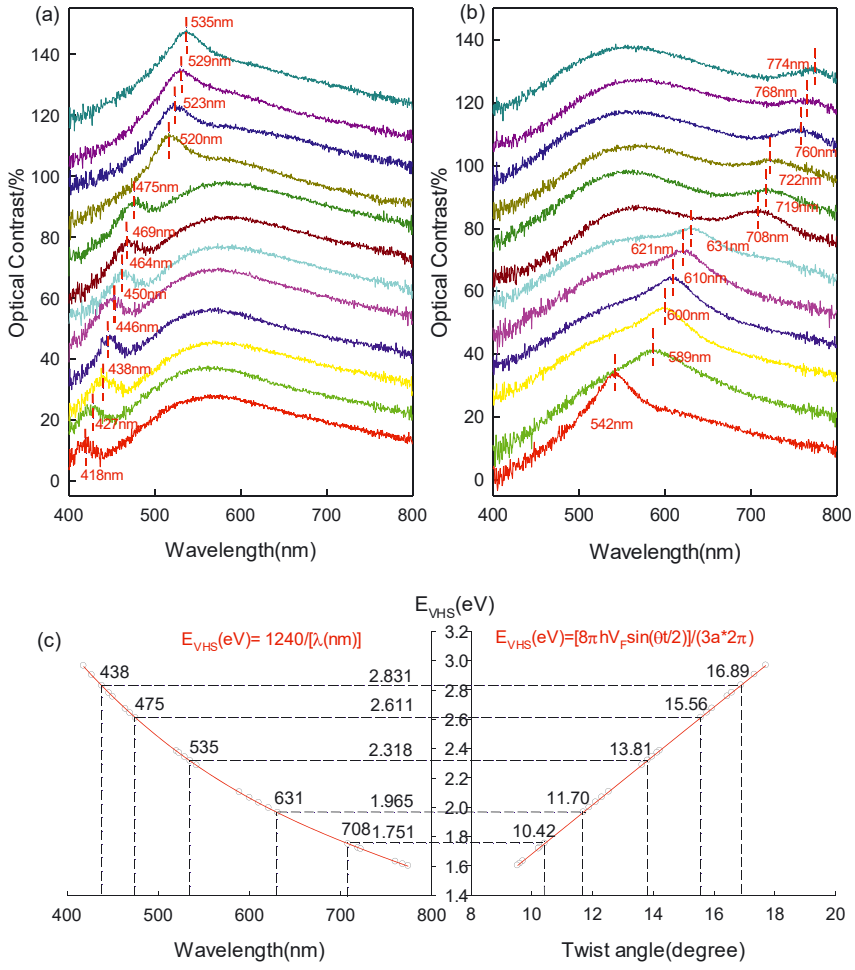

Figure 2: (a) the optical contrast of 12 tBLGs with different absorption peak wavelength of 418–535 nm, (b) the optical contrast of 12 tBLGs with different absorption peak wavelength of 542–774 nm. (c) The wavelength of absorption peak of 24 tBLGs were converted to E_{VHS}, and their θ_t were calculated by E_{VHS}.

showed the θ_t of all 24 tBLGs were between 9 and 18° by using the calculated results of E_{VHS} as a function of θ_t, which can be seen in Figure 2c. The wavelength of absorption peak corresponds to a unique energy of E_{VHS} and a unique twist angle θ_t. Therefore, as shown in the black hollow points in Figure 2c, the absorption peak of OC(λ) relates to the θ_t of tBLG, and each peak corresponds to an angle. For example, the absorption peak at 708 nm corresponds to 1.751 eV of E_{VHS} and 10.42° of θ_t, the absorption peak at 631 nm corresponds to 1.965 eV of E_{VHS} and 11.70° of θ_t, the absorption peak at 535 nm corresponds to 2.318 eV of E_{VHS} and 13.81° of θ_t, the absorption peak at 475 nm corresponds to 2.611 eV of E_{VHS} and 15.56° of θ_t, the absorption peak at 438 nm corresponds to 2.831 eV of E_{VHS} and 16.89° of θ_t, and so on.

3.3 The relationship between the absorption peak in OC(λ) and the G-mode resonance in Raman spectra

In addition to the θ_t-dependent absorption behavior, resonance Raman spectroscopy of G band can provide evidence of θ_t-dependent electronic and optical properties in tBLG [18–21]. To further understand the relation of the G-mode resonance in Raman spectra with the absorption peak in OC(λ), the G modes of 24 tBLGs mentioned in Figure 2 were measured. Figure 3 shows the G mode intensities as a function of OC absorption peaks at the excitation of six lasers of 2.71, 2.54, 2.33, 2.09, 1.96, and 1.83 eV. (The data of different lasers are shown in different colors). Here, the energy of absorption peak of tBLGs (E_{VHS}) were determined as *x*-axis, the G mode intensities (I(G)) of tBLGs as *y*-axis were calibrated with the Si mode intensity (I(Si)) of themselves and were recorded as I(G)/I(Si). Among them, the dots represent experimental data, while solid lines are Gaussian fitting lines based on experimental results. It can be clearly seen that the enhancement of the G-band intensity occurs in tBLGs with different lasers. The I(G)/I(Si) appears maximum when E_{VHS} approximates to E_L (the energy of the excitation laser). For example, Figure 3a shows the value of I(G)/I(Si) reaches up to about 80 times the value of non-resonant I(G)/I(Si) at E_{VHS} of 2.709 eV which matches E_L of 2.71 eV, Figure 3c shows the value of I(G)/I(Si) reaches up to about 65 times the value of non resonant I(G)/I(Si) at E_{VHS} of 2.285 eV which matches E_L of 2.33 eV, Figure 3d shows the value of I(G)/I(Si) reaches up to about 40 times the value of non-resonant I(G)/I(Si) at E_{VHS} of 2.065 eV which matches E_L of 2.09 eV, and so on. These results show that the G band enhancement has universal, one-to-one correspondence with OC absorption enhancement for tBLGs. (Raman spectra of 1480–1680 cm^{-1} containing G modes of 24 tBLGs measured by these six lasers are shown in Figure S2 of Supplementary Materials.)

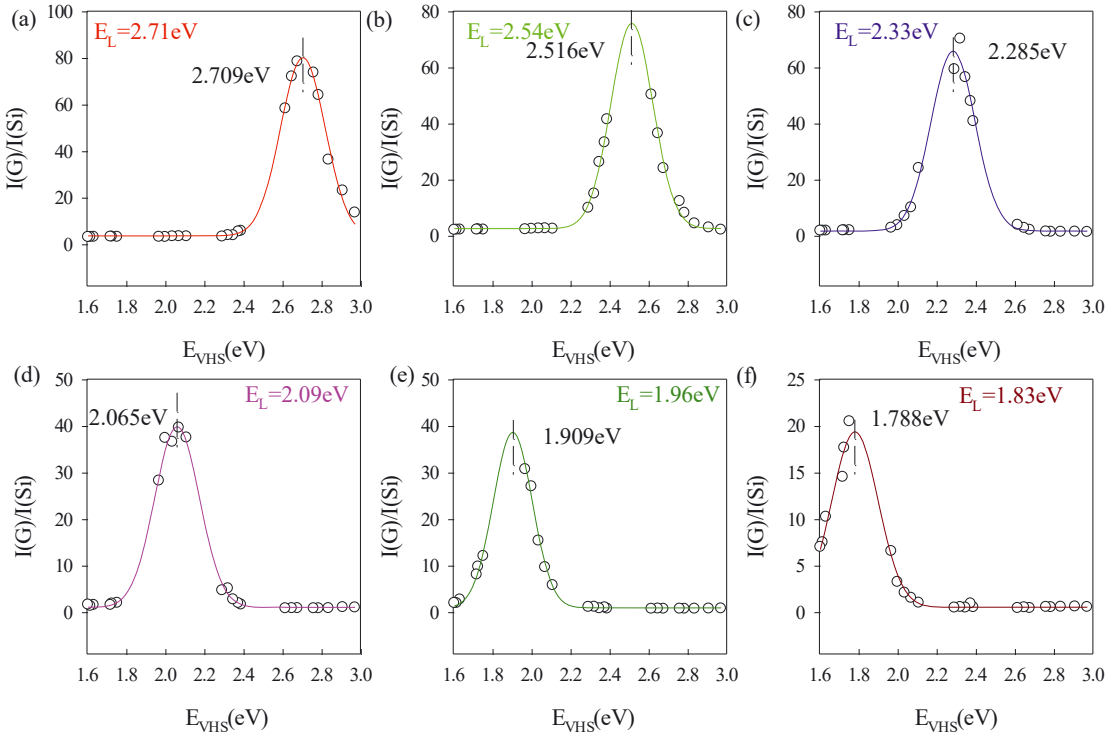

Figure 3: The I(G)/I(Si) of 24 tBLGs as a function of E_{VHS} of tBLGs measured by six lasers with E_L of 2.71, 2.54, 2.33, 2.09, 1.96, and 1.83 eV.

Because the band structure of tBLG is significantly affected by the presence of a twisted interface, parallel conduction and valence bands along the K–M direction will appear when there is a twist angle between two layers. Only the optically allowed electronic transitions can be involved in the resonant Raman process of G mode [19]. The corresponding optically allowed joint density of states JDOS (called as $\mathrm{JDOS_{OAT}}$) in tBLGs can be calculated by the following equation [9]:

$$\mathrm{JDOS_{OAT}}(E) \propto \sum_{ij}\sum_{k}\left|M_{ij}(k)\right|^2\delta\left(E_{ij}(k)-E\right)$$

where $M_{ij}(k)$ is the optical matrix element between the ith conduction and jth valence bands and $E_{ij}(k)$ gives the transition energy of an i–j band pair at the wavevector k. $\mathrm{JDOS_{OAT}}$ occurs at E equal to E_{VHS} due to new singularities in JDOS of tBLGs. The intensity of G mode in tBLGs as a function of E_{L} can be evaluated as [8, 22]:

$$A \propto \left|\sum_{j}\frac{M_j}{(E_{\mathrm{L}}-E_{\mathrm{VHS}}(j)-i\gamma)(E_{\mathrm{L}}-E_{\mathrm{ph}}-E_{\mathrm{VHS}}(j)-i\gamma)}\right|^2$$

where M_j are constants treated as fitting parameters that encompass the product of the electron–phonon and electron–photon interactions matrix elements for the jth valence bands related to VHSs in the $\mathrm{JDOS_{OAT}}$, E_{ph} is the phonon energy (0.196 eV for G mode) and γ gives the energy uncertainty related to the lifetime of the excited state. When E_{L}

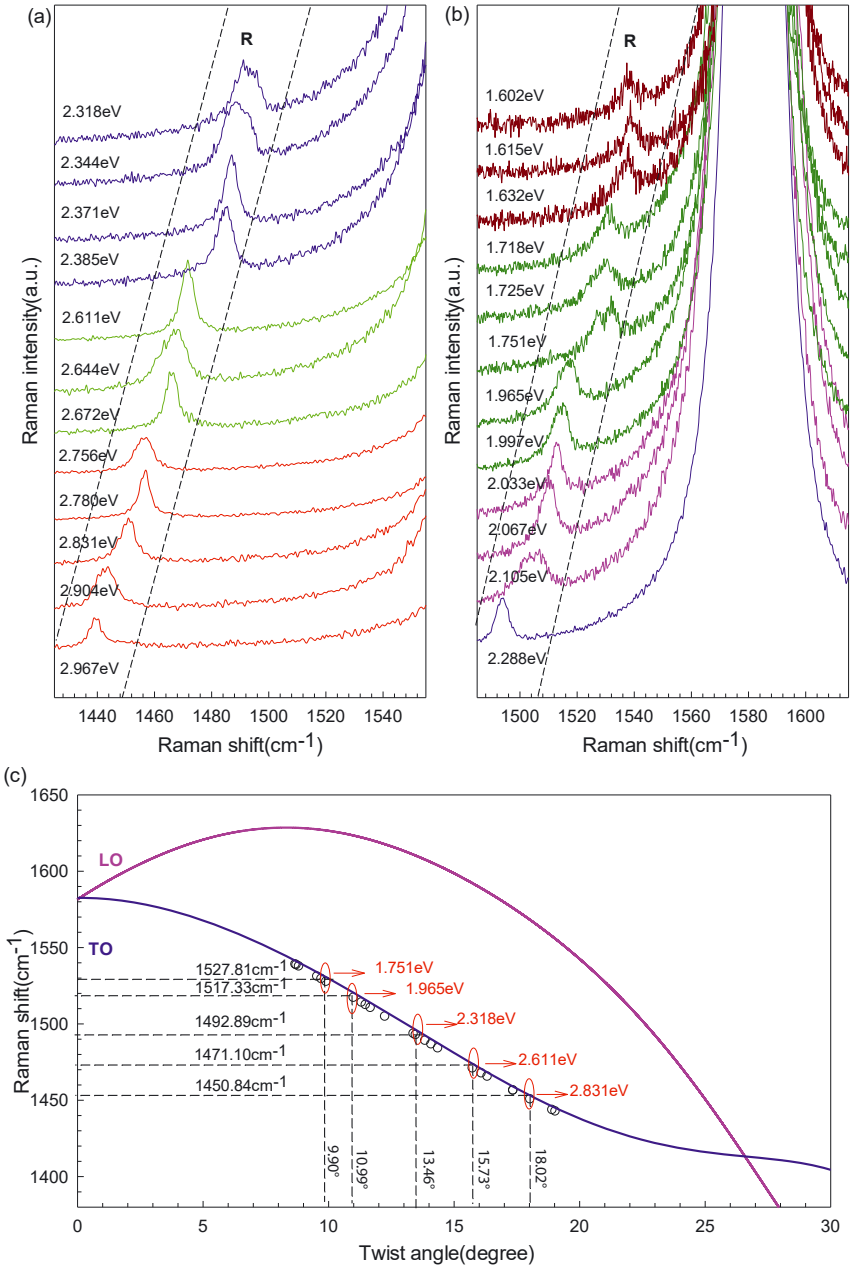

Figure 4: (a) The R mode of 12 tBLGs with E_{VHS} of 2.318–2.967 eV, (b) the R mode of 12 tBLGs with E_{VHS} of 1.602–2.288 eV. (c) The θ_{t} of 24 tBLGs were calculated by TO phonon branch (reported by G. S. N. Eliel et al. [26]).

is close to E_{VHS}, the intensity of the G mode is significantly enhanced. Thus, the G-mode resonance in Raman spectra and the absorption peak in OC(λ) are related by E_{VHS}.

3.4 The relationship between the R-mode in Raman spectra and twist angle θ_t

In addition, two new Raman features (R and R′ modes) [8, 23, 24] appear in the tBLGs in principle as a result of intravalley and intervalley double resonance processes involving elastic electron scattering by the static potential which stems from the interaction between the two layers. These phonons are away from the center of Brillouin zone, which are selected by the twist wavevector $q(\theta_t)$. The R and R′ modes are located below and above the G-band position, respectively, since the R mode originates from the TO phonon branch and is activated by the interlayer interaction process and the R′ mode originates from the LO phonon branch and is activated by the intralayer interaction process [23]. However, the R and R′ modes are difficult to be measured due to their low intensity. Particularly, the R′ band is unlikely to be observed for larger angles since its strength is drastically reduced for the LO phonon branch [8]. Moreover, the R′ band is easily confused with the D′ band, which is also located above the G band and is activated by defect induced intravalley double resonance Raman process [25] if there are some defects in graphene. Here, we focus on the R modes of the 24 tBLGs mentioned in Figure 2. Figure 4a and b show the R modes of tBLGs excited by lasers of 2.71, 2.54, 2.33, 2.09, 1.96, and 1.83 eV. The data of different lasers are shown in different colors, which are consistent with the color representation in Figure 3. As shown in Figure 4a and b, the R modes are at the low energy side of the G mode and are highlighted in black dotted area. It is noting that the R modes of tBLGs with different absorption peak energy can just be observed in a small resonant window under resonance conditions of matching E_L with E_{VHS} as reported in Ref. [8]. For example, the R modes in tBLGs with E_{VHS} from 2.967 to 2.756 eV were measured with the laser of 2.71 eV, as indicated by red lines in Figure 4a, the R modes in tBLGs with E_{VHS} from 2.672 to 2.611 eV were measured with the laser of 2.54 eV, as indicated by green lines in Figure 4a, the R modes in tBLGs with E_{VHS} from 2.385 to 2.288 eV were measured with the laser of 2.33 eV, as indicated by blue lines in Figure 4a and b, the R modes in tBLGs with the absorption peak energy from 2.105 to 2.033 eV were measured with the laser of 2.09 eV, as indicated by pink lines in Figure 4b, the R modes in tBLGs with the absorption peak energy from 1.997 to 1.718 eV were measured with the laser of 1.96 eV, as indicated by dark green lines in Figure 4b, the R modes in tBLGs with the absorption peak energy from 1.632 to 1.602 eV were measured with the laser of 1.83 eV, as indicated by brown lines in Figure 4b. Thus, the R-mode resonance in Raman spectra and the optical absorption peak in OC(λ) are also related by E_{VHS}.

The θ_t in tBLGs can be derived from the observed R modes. Figure 4c shows the relation between R mode and θ_t. The blue line is TO phonon branch of tBLG as a function of θ_t, which is the theoretical calculation result of R mode reported by G. S. N. Eliel et al. [26]. The black hollow points are picked out to accord with the measured R mode frequencies of 24 tBLGs. The θ_t of all 24 tBLGs were between 8° and 20°, which can be seen in Figure 4c. For example, the R mode at 1527.81 cm^{-1} corresponds to θ_t as 9.90° and E_{VHS} as 1.751 eV, the R mode at 1517.33 cm^{-1} corresponds to θ_t as 10.99° and E_{VHS} as 1.965 eV, the R mode at 1492.89 cm^{-1} corresponds to θ_t as 13.46° and E_{VHS} as 2.318 eV, the R mode at 1471.10 cm^{-1} corresponds to θ_t as 15.73° and E_{VHS} as 2.611 eV, the R mode at 1450.84 cm^{-1} corresponds to θ_t as 18.02° and E_{VHS} as 2.831 eV, and so on.

In this case, we listed the twist angles obtained from the R mode (denoted as θ_R) and from the OC absorption peak (denoted as θ_{OC}) in Table 1. Please note that the error

Table 1: The wavelength of absorption peak, the corresponding E_{VHS}, the twist angle obtained from the OC absorption peak θ_{OC}, the twist angles obtained from the R mode θ_R, and the error between θ_R and θ_{OC}.

Absorption peak wavelength (nm)	E_{VHS} (eV)	θ_{OC} (°)	R mode frequency (cm^{-1})	θ_R (°)	$(\theta_{OC} - \theta_R)/\theta_{OC} \times 100\%$
418	2.967	17.70	1442.86	19.03	−7.49%
427	2.904	17.33	1443.82	18.90	−9.10%
438	2.831	16.89	1450.84	18.02	−6.74%
446	2.780	16.58	1456.59	17.35	−4.60%
450	2.756	16.43	1456.59	17.34	−5.54%
464	2.672	15.93	1465.67	16.32	−2.42%
469	2.644	15.76	1467.84	16.08	−2.03%
475	2.611	15.56	1471.10	15.73	−1.07%
520	2.385	14.21	1484.23	14.35	−0.98%
523	2.371	14.13	1486.82	14.08	0.32%
529	2.344	13.97	1489.21	13.84	0.92%
535	2.318	13.81	1492.89	13.46	2.51%
542	2.288	13.63	1493.75	13.38	1.87%
589	2.105	12.54	1504.98	12.24	2.38%
600	2.067	12.31	1510.70	11.66	5.25%
610	2.033	12.10	1512.61	11.47	5.27%
621	1.997	11.90	1514.19	11.31	4.90%
631	1.965	11.70	1517.33	10.99	6.11%
708	1.751	10.42	1527.81	9.90	5.06%
719	1.725	10.26	1529.64	9.70	5.47%
722	1.718	10.22	1531.21	9.54	6.71%
760	1.632	9.71	1537.85	8.81	9.27%
768	1.615	9.61	1538.73	8.71	9.35%
774	1.602	9.53	1539.11	8.67	9.08%

between θ_R and θ_{OC} is basically less than 7% except for the OC absorption peak wavelength shorter than 438 nm or larger than 760 nm. In summary, the θ_t of tBLG were investigated by using both OC and Raman spectroscopy. The variation of OC absorption peak wavelength with twist angle is essentially a reflection of the variation of electronic band structure with twist angle in tBLGs. However, the variation of R-mode frequency with the twist angle is caused by phonon folding in the Morie superlattice, that is, the twist angle is related to the phonon dispersion. Thus, the twist angles obtained by two methods in the same tBLG showed a little different. In addition, both methods could produce some errors during experiments. Because the absorption peak of OC was not symmetric in the first method, there might be some errors when we took the position of the maximum of the absorption peak as E_{VHS} to obtain the value of twist angle. In the other method, the measured R-modes were much weaker than G-modes and there existed some asymmetrical broadenings. There might be some errors when we used the frequency of the maximum of R-mode to obtain the value of twist angle.

4 Conclusion

Due to the novel electronic states caused by twist angle of tBLG, absorption peak appears in OC of tBLG whose energy is closely related to E_{VHS} in JDOS. Furthermore, the Raman G mode and R mode are significantly enhanced at E_{VHS}. The relation between these optical properties and E_{VHS} are established, which gives a viable method in identifying the twist angle in tBLG. The results of θ_t obtained by OC absorption peak are consistent with those by the Raman R mode. It shows that the results of θ_t deduced from the OC absorption peak are reliable and this method can be used to identify twist angles of tBLGs. Our findings provide evidence of coherent interactions between the states associated with the low-energy VHSs in tBLG and will contribute to the further research of twist angle dependent characteristics of novel optical and optoelectronic tBLG devices.

Acknowledgments: This work is supported by Natural Science Foundation of People's Republic of China (12004376), Hebei Province Natural Science Foundation (A2020201028), Postgraduate Innovation Project of Hebei University (HBU2021ss069).
Author contribution: All the authors have accepted responsibility for the entire content of this submitted manuscript and approved submission.
Research funding: None declared.
Competing interests: The authors declare that they have no competing interests.

References

[1] I. V. Antonova, "Chemical vapor deposition growth of graphene on copper substrates: current trends," *Phys. Usp.*, vol. 56, pp. 1013–1020, 2013.
[2] R. Bistritzer, and A. H. MacDonald, "Moire bands in twisted double-layer graphene," *Proc. Natl. Acad. Sci. U.S.A.*, vol. 108, pp. 12233–12237, 2011.
[3] Y. Hou, X. B. Ren, J. C. Fan, et al., "Preparation of twisted bilayer graphene via the wetting transfer method," *ACS Appl. Mater. Interfaces*, vol. 12, pp. 40958–40967, 2020.
[4] J. M. B. L. dos Santos, N. M. R. Peres, and A. H. Castro Neto, "Graphene bilayer with a twist: electronic structure," *Phys. Rev. Lett.*, vol. 99, p. 256802, 2007.
[5] G. H. Li, A. Luican, J. M. B. L. dos Santos, et al., "Observation of Van Hove singularities in twisted graphene layers," *Nat. Phys.*, vol. 6, pp. 109–113, 2010.
[6] Y. Cao, V. Fatemi, A. Demir, et al., "Correlated insulator behaviour at half-filling in magic-angle graphene superlattices," *Nature*, vol. 556, p. 80, 2018.
[7] Y. Cao, V. Fatemi, S. Fang, et al., "Unconventional superconductivity in magic-angle graphene superlattices," *Nature*, vol. 556, p. 43, 2018.
[8] V. Carozo, C. M. Almeida, B. Fragneaud, et al., "Resonance effects on the Raman spectra of graphene superlattices," *Phys. Rev. B*, vol. 88, 2013, Art no. 085401.
[9] J. B. Wu, X. Zhang, M. Ijaes, et al., "Resonant Raman spectroscopy of twisted multilayer graphene," *Nat. Commun.*, vol. 5, p. 5309, 2014.
[10] R. W. Havener, Y. F. Liang, L. Brown, L. Yang, and P. J. Van Hove, "Singularities and excitonic effects in the optical conductivity of twisted bilayer graphene," *Nano Lett.*, vol. 14, pp. 3353–3357, 2014.
[11] K. Yu, N. V. Luan, T. Kim, et al., "Gate tunable optical absorption and band structure of twisted bilayer graphene," *Phys. Rev. B*, vol. 99, p. 241405, 2019.
[12] P. Moon, and M. Koshino, "Optical absorption in twisted bilayer graphene," *Phys. Rev. B*, vol. 87, p. 205404, 2013.
[13] W. J. Zhao, P. H. Tan, J. Zhang, and J. A. Liu, "Charge transfer and optical phonon mixing in few-layer graphene chemically doped with sulfuric acid," *Phys. Rev. B*, vol. 82, p. 245423, 2010.
[14] Z. H. Ni, H. M. Wang, J. Kasim, et al., "Graphene thickness determination using reflection and contrast spectroscopy," *Nano Lett.*, vol. 7, pp. 2758–2763, 2007.
[15] J. Wang, W. Bo, Y. Ding, X. Wang, and X. Mu, "Optical, optoelectronic, and photoelectric properties in moire superlattices of twist bilayer graphene," *Mater. Today Phys.*, vol. 14, p. 100238, 2020.
[16] P. Moon, and M. Koshino, "Energy spectrum and quantum Hall effect in twisted bilayer graphene," *Phys. Rev. B*, vol. 85, p. 195458, 2012.

[17] H. B. Ribeiro, K. Sato, G. S. N. Eliel, et al., "Origin of van Hove singularities in twisted bilayer graphene," *Carbon*, vol. 90, pp. 138–145, 2015.
[18] G. S. N. Eliel, H. B. Ribeiro, K. Sato, et al., "Raman excitation profile of the G-band enhancement in twisted bilayer graphene," *Braz. J. Phys.*, vol. 47, pp. 589–593, 2017.
[19] R. W. Havener, H. L. Zhuang, L. Brown, R. G. Hennig, and J. Park, "Angle-resolved Raman imaging of inter layer rotations and interactions in twisted bilayer graphene," *Nano Lett.*, vol. 12, pp. 3162–3167, 2012.
[20] K. Sato, R. Saito, C. X. Cong, T. Yu, and M. S. Dresselhaus, "Zone folding effect in Raman G-band intensity of twisted bilayer graphene," *Phys. Rev. B*, vol. 86, p. 125414, 2012.
[21] Z. H. Ni, L. Liu, Y. Y. Wang, et al., "G-band Raman double resonance in twisted bilayer graphene: evidence of band splitting and folding," *Phys. Rev. B*, vol. 80, p. 125404, 2009.
[22] E. Koo, S. Kim, and S. Y. Ju, "Relationships between the optical and Raman behavior of van Hove singularity in twisted bi- and fewlayer graphenes and environmental effects," *Carbon*, vol. 111, pp. 238–247, 2017.
[23] V. Carozo, C. M. Almeida, E. H. M. Ferreira, L. G. Cancado, C. A. Achete, and A. Jorio, "Raman signature of graphene superlattices," *Nano Lett.*, vol. 11, pp. 4527–4534, 2011.
[24] C. C. Lu, Y. C. Lin, Z. Liu, C. H. Yeh, K. Suenaga, and P. W. Chiu, "Twisting bilayer graphene superlattices," *ACS Nano*, vol. 7, pp. 2587–2594, 2013.
[25] J. F. Rodriguez-Nieva, E. B. Barros, R. Saito, and M. S. Dresselhaus, "Disorder-induced double resonant Raman process in graphene," *Phys. Rev. B*, vol. 90, p. 235410, 2014.
[26] G. S. N. Eliel, M. V. O. Moutinho, A. C. Gadelha, et al., "Intralayer and interlayer electron-phonon interactions in twisted graphene heterostructures," *Nat. Commun.*, vol. 9, p. 1221, 2018.

Supplementary Material: The online version of this article offers supplementary material (https://doi.org/10.1515/nanoph-2021-0190).